The First Direct Characterization of a High-Valent Iron Intermediate in the Reaction of an α-Ketoglutarate-Dependent Dioxygenase: A High-Spin Fe(IV) Complex in Taurine/α-Ketoglutarate Dioxygenase (TauD) from *Escherichia coli*†

John C. Price, Eric W. Barr, Bhramara Tirupati, J. Martin Bollinger, Jr.,* and Carsten Krebs*

Department of Biochemistry and Molecular Biology, The Pennsylvania State University, University Park, Pennsylvania 16802

Received January 10, 2003; Revised Manuscript Received April 4, 2003

ABSTRACT: The Fe(II)- and α-ketoglutarate(αKG)-dependent dioxygenases have roles in synthesis of collagen and sensing of oxygen in mammals, in acquisition of nutrients and synthesis of antibiotics in microbes, and in repair of alkylated DNA in both. A consensus mechanism for these enzymes, involving (i) addition of O_2 to a five-coordinate, $(His)_2(Asp)$-facially coordinated Fe(II) center to which αKG is also bound via its C-1 carboxylate and ketone oxygen; (ii) attack of the uncoordinated oxygen of the bound O_2 on the ketone carbonyl of αKG to form a bicyclic Fe(IV)-peroxyhemiketal complex; (iii) decarboxylation of this complex concomitantly with formation of an oxo-ferryl ($Fe(IV)=O^{2-}$) intermediate; and (iv) hydroxylation of the substrate by the $Fe(IV)=O^{2-}$ complex via a substrate radical intermediate, has repeatedly been proposed, but none of the postulated intermediates occurring after addition of O_2 has ever been detected. In this work, an oxidized Fe intermediate in the reaction of one of these enzymes, taurine/α-ketoglutarate dioxygenase (TauD) from *Escherichia coli*, has been directly demonstrated by rapid kinetic and spectroscopic methods. Characterization of the intermediate and its one-electron-reduced form (obtained by low-temperature γ-radiolysis of the trapped intermediate) by Mössbauer and electron paramagnetic resonance spectroscopies establishes that it is a high-spin, formally Fe(IV) complex. Its Mössbauer isomer shift is, however, significantly greater than those of other known Fe(IV) complexes, suggesting that the iron ligands in the TauD intermediate confer significant Fe(III) character to the high-valent site by strong electron donation. The properties of the complex and previous results on related αKG-dependent dioxygenases and other non-heme-Fe(II)-dependent, O_2-activating enzymes suggest that the TauD intermediate is most probably either the Fe(IV)-peroxyhemiketal complex or the taurine-hydroxylating $Fe(IV)=O^{2-}$ species. The detection of this intermediate sets the stage for a more detailed dissection of the TauD reaction mechanism than has previously been reported for any other member of this important enzyme family.

The Fe(II)/α-ketoglutarate-dependent dioxygenases couple oxidative decarboxylation of α-ketoglutarate (2-oxo-1,5-pentanedioic acid, hereafter denoted αKG[1]) with hydroxylation of unactivated carbon atoms on a variety of substrates. Enzymes belonging to this class catalyze numerous metabolically important reactions in organisms from bacteria to man (*1*−*3*). Many of these reactions have particular medical, pharmaceutical, or environmental relevance. For example, key steps in the biosyntheses of the important antibiotics penicillin (*4*), cephalosporin (*5*), and vancomycin (*6*) are catalyzed by members of the αKG-dependent dioxygenase family. In mammals, reactions necessary for cross-linking of collagen and for the detection of oxygen and response to hypoxia are catalyzed by enzymes in this class (*7*−*10*). Very recently, αKG-dependent dioxygenases have been shown to participate in DNA repair processes in both bacteria (*11*) and humans (*12*). In addition, defects in enzymes of this family have been associated with several disease states (*3*), such as alcoholic liver cirrhosis (*13*, *14*), Ehlers-Danlos syndrome (*13*), hawkinsinuria (*15*, *16*), and Refsum's disease (*16*). The number of recognized members of this family has grown rapidly in the past few years, and sequencing projects promise to continue to fuel this explosive growth. For example, the genome of *Arabidopsis thaliana* was found to contain 64 previously uncharacterized open reading frames encoding potential members (*2*).

Recent reviews (*1*, *17*) would suggest that consensus has been reached on a general reaction mechanism for these enzymes (Scheme 1 shows this mechanism adapted for the specific case of TauD, the subject of this work). The basic tenets of the mechanism are (i) binding of αKG via its C-1 carboxylate and ketone oxygens to the Fe(II) center of the

† This work was supported by start-up funds from the Pennsylvania State University (C.K.) and a seed grant from the Innovative Biotechnology Research Fund of the Huck Institute for Life Sciences at the Pennsylvania State University (J.M.B. and C.K.).

* To whom correspondence should be addressed: Please send correspondence to J. Martin Bollinger, Jr., Department of Biochemistry and Molecular Biology, 208 Althouse Laboratory, University Park, PA 16802. Phone: 814-863-5707. Fax: 814-863-7024. E-mail: jmb21@psu.edu. Carsten Krebs, Department of Biochemistry and Molecular Biology, 306 S. Frear Bldg., University Park, PA 16802. Phone: 814-865-6089. Fax: 814-863-7024. E-mail: ckrebs@psu.edu.

[1] Abbreviations: TauD, taurine/α-ketoglutarate dioxygenase; αKG, α-ketoglutarate or 2-oxo-1,5-pentanedioic acid; δ, Mössbauer isomer shift; ΔE_Q, Mössbauer quadrupole splitting; ϵ, molar absorptivity; $\Delta\epsilon$, change in molar absorptivity relative to that of the reactant complex.

10.1021/bi030011f CCC: $25.00 © 2003 American Chemical Society
Published on Web 05/28/2003

Scheme 1: Working Hypothesis for the Mechanism of Taurine Hydroxylation Catalyzed by TauD

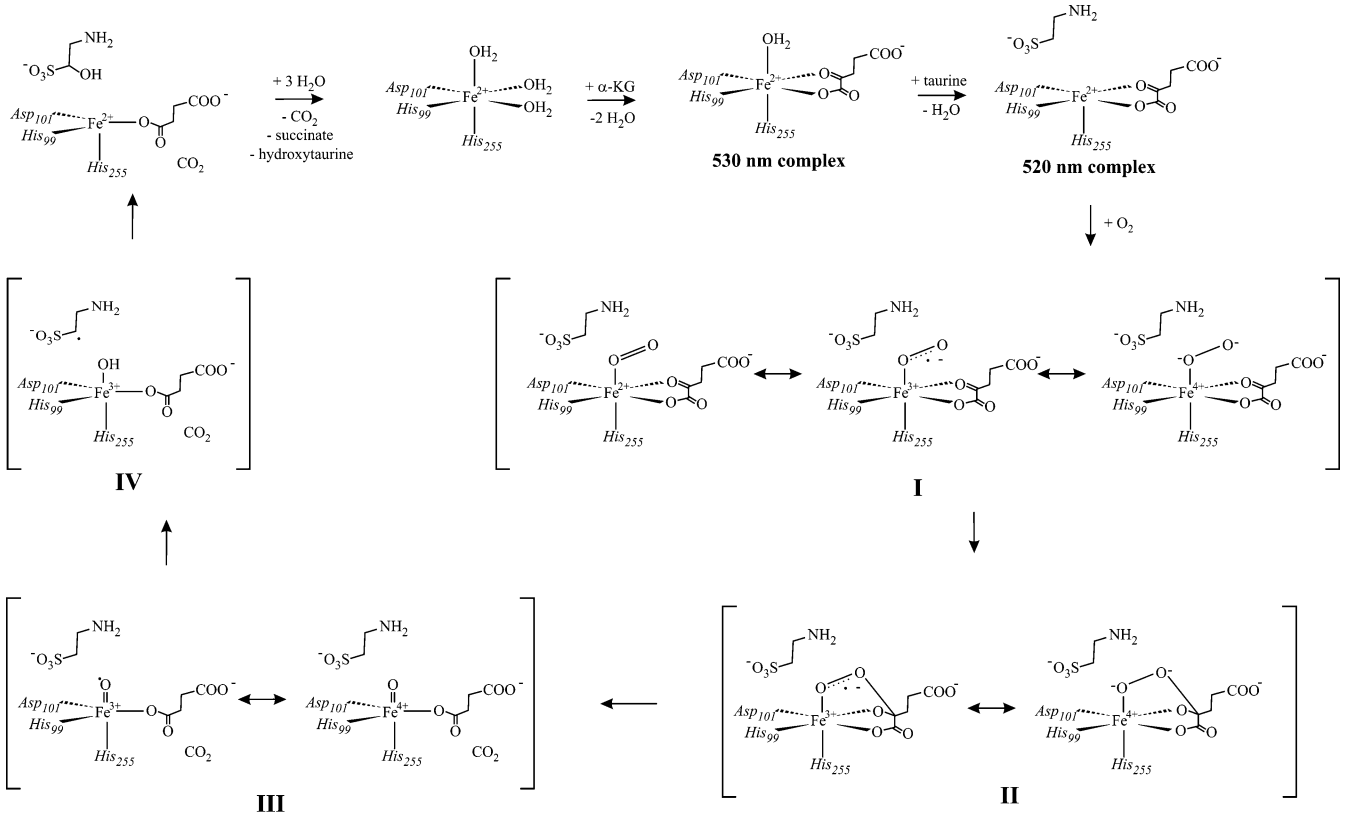

binary enzyme·Fe(II) complex, with displacement of two water ligands (forming the 530 nm complex in Scheme 1); (ii) binding of the substrate in the vicinity of the Fe(II) center, with formation of a five-coordinate Fe(II) site by dissociation of a third coordinated water molecule (the 520 nm complex in Scheme 1); (iii) binding of dioxygen end-on to the open coordination site on the Fe(II) (complex **I**); (iv) attack of the uncoordinated oxygen atom of O_2 on the carbonyl of αKG, leading to its oxidative decarboxylation to succinate concomitantly with formation of an oxo-ferryl ($Fe(IV)=O^{2-}$) intermediate (complex **III**); and (v) hydroxylation of the substrate by the $Fe(IV)=O^{2-}$ species by a mechanism that might be similar to that employed by the heme-dependent cytochromes P-450. Despite the apparent consensus, no direct demonstration of any of the intermediate species after the quaternary enzyme·Fe(II)·αKG·substrate complex has, to our knowledge, been reported for any enzyme in this class.

Taurine/α-ketoglutarate dioxygenase (TauD) from *Escherichia coli* catalyzes the hydroxylation of taurine (2-amino-1-ethanesulfonic acid) and other sulfonic acids at C-1. This reaction initiates the elimination of sulfite and thereby allows the bacterium to acquire sulfur from organic sulfonates (*18*). By comparison of kinetic, spectroscopic, and structural data on TauD with those on other αKG-dependent dioxygenases and inorganic model complexes, Hausinger and co-workers delineated several important features of the TauD reaction cycle (*19*, *20*). They demonstrated that, as in other enzymes in the family, binding of αKG to the binary enzyme·Fe(II) complex gives rise to a weak optical absorption band ($\lambda_{max} = 530$ nm, $\epsilon_{530} \sim 180$ M^{-1} cm^{-1}). Previous studies on the cognate complex of another enzyme in the family had shown that this absorption feature arises from a metal-to-ligand charge-transfer transition associated with coordination of the αKG ketone carbonyl (*21*, *22*). Resonance Raman data on the TauD·Fe(II)·αKG complex and inorganic models for it were consistent with this assignment (*20*). Hausinger and co-workers also showed that taurine binds synergistically with αKG (decreasing the apparent dissociation constant for αKG from 350 μM in the absence of taurine to 6 μM in the presence of 2 mM taurine) and that its binding slightly blue-shifts the metal-to-ligand charge-transfer band to $\lambda_{max} = 520$ nm. Resonance Raman data were consistent with conversion from a six-coordinate to a five-coordinate Fe(II) site upon binding of taurine (*20*), and X-ray crystallographic data provided support for the presence of five-coordinate Fe(II) in the quaternary complex (*23*). These results would imply that, in TauD, as in other enzymes in this family, the binding of substrate (taurine) serves as a conformational trigger for oxygen activation. Consistent with this notion, Ryle et al. found that the TauD·Fe(II)·αKG ternary complex reacts much less rapidly with O_2 than does the TauD·Fe(II)·αKG·taurine quaternary complex, as determined by the loss of the visible chromophore upon mixing with O_2 (*19*).

The simplicity of its substrate, the relative ease with which it can be prepared in large quantity, its stability, and its recent crystallographic characterization (*23*) make TauD particularly attractive among members of the Fe(II)/αKG-dependent dioxygenase family as a candidate for mechanistic dissection. Herein we report stopped-flow absorption and freeze-quench Mössbauer and EPR experiments that directly demonstrate the accumulation of a kinetically competent, oxidized iron intermediate after addition of dioxygen to the quaternary TauD·Fe(II)·αKG·taurine complex. On the basis of the Mössbauer and EPR characteristics of the intermediate and its one-electron-cryoreduced form, we conclude that it is a

high-spin, formally Fe(IV) species with substantial delocalization of the oxidizing equivalent onto the ligands.

MATERIALS AND METHODS

Materials. DNA modifying enzymes and reagents for the polymerase chain reaction (PCR) were purchased from New England Biolabs (Beverly, MA). Oligonucleotide primers were purchased from Invitrogen (Carlsbad, CA). DNA sequence determinations were performed by the Nucleic Acid Facility of the Penn State University Biotechnology Institute. *E. coli* strain BL21(DE3) and the vector pET22b were purchased from Novagen (Madison, WI). *E. coli* strain DH5α was purchased from PGC Scientific (Gaithersburg, MD). Culture media components (yeast extract and tryptone) were purchased from Marcor Development Corporation (Hackensack, NJ). Isopropyl-*β*-D-thiogalactopyranoside (IPTG) was purchased from Biosynth International (Naperville, IL). Ampicillin was purchased from IBI (Shelton, CT). 5,5′-Dithio-bis-(2-nitrobenzoic acid) (Ellman's reagent) was purchased from Pierce (Rockford, IL). Glycerol, ammonium sulfate, sodium chloride, ferrous ammonium sulfate, and sodium hydroxide were purchased from EM Science (Gibbstown, NJ). Trizma (Tris) base, 2-amino-ethanesulfonic acid (taurine), 2-oxo-glutarate (αKG), sodium sulfite, imidazole, poly(ethyleneimine), ethylenediaminetetraacetic acid (EDTA), and 2-methylbutane were purchased from Sigma Corp. (St. Louis, MO). Trichloroacetic acid and sulfuric acid were purchased from Fisher Scientific (Pittsburgh, PA). Dithiothreitol (DTT) was purchased from USB Corp. (Cleveland, OH). DEAE-Sepharose FF resin was purchased from Pharmacia (Piscataway, NJ). ^{57}Fe metal was purchased from Advanced Materials and Technology (New York, NY).

Construction of TauD Overexpression Strain. An 878-bp DNA fragment containing the *tauD* gene was amplified by PCR by using a suspension of *E. coli* strain JM109 as template and primers, "forward" (5′-GGAGAAGTCATATGAGTGAACG-3′) and "reverse" (5′-CCGTCCACTCTCGAGTTACCCC-3′). The PCR fragment was restricted with *Nde*I (site underlined in "forward") and *Xho*I (underlined in "reverse") and ligated with pET22b that had been restricted with the same endonucleases. The ligation solution was used to transform *E. coli* DH5α to ampicillin resistance. The entire TauD coding sequence from a plasmid (pTauD) isolated from one transformant was verified. This plasmid was then used to transform the expression strain, *E. coli* BL21(DE3).

Overexpression of TauD. BL21(DE3)/pTauD cells were grown in enriched medium (35 g/L tryptone, 20 g/L yeast extract, 5 g/L NaCl, brought to pH 7.3 with NaOH and supplemented with 150 mg/L ampicillin) while shaking vigorously in Fernbach flasks at 37 °C to an optical density at 600 nm of 0.6−1. Cultures were cooled on ice for 15 min and then induced to overexpress TauD by addition of IPTG to 0.2 mM. After induction, cultures were shaken at 16 °C for an additional 24 h. The cells were then harvested at 4 °C by centrifugation at 10000*g* for 10 min. A typical yield was 16 g of wet cell mass per L of culture. The cell paste was either used immediately for protein purification or was frozen in liquid nitrogen and stored at −80 °C prior to being used.

Purification of TauD. All purification steps were carried out at 4 °C. In a representative purification, 107 g of cell paste was resuspended in 500 mL of buffer A (50 mM Tris·HCl, pH 7.6, containing 10% (v/v) glycerol). The cells were lysed by a single passage through a French pressure cell at 16 000 psi. Following centrifugation of the lysate at 16000*g* for 10 min, 0.05 volume equivalents of a 10% solution of poly(ethyleneimine) in buffer A was added to the supernatant slowly with continuous stirring. The resulting suspension was centrifuged at 16000*g* for 10 min. The supernatant was brought to 60% of saturation in ammonium sulfate by slow addition of the solid with continuous stirring. The resulting suspension was centrifuged at 16000*g* for 10 min, and the pellet (29.1 g) was redissolved in buffer A (108 mL) containing 1 mM sodium EDTA and 1 mM dithiothreitol. The protein solution was then dialyzed twice against 2 L of this buffer. The dialysate was loaded onto a 1 L DEAE-Sepharose FF column in buffer A. The column was washed first with 1 L of buffer A and then with a 750 mL linear gradient of 0−0.05 M NaCl in buffer A. The protein was eluted with a 2.25 L linear gradient of 0.05−0.2 M NaCl in buffer A. Fractions containing TauD were pooled and concentrated to ∼3 mM in an Amicon Diaflow stirred pneumatic concentrator with a YM-30 membrane. The protein was dialyzed twice against 4 L of buffer A, flash-frozen in liquid nitrogen, and stored at −80 °C. The protein was estimated to be greater than 95% pure by denaturing polyacrylamide gel electrophoresis and Coomassie staining. The concentration of TauD was determined by absorbance at 280 nm by using the molar absorptivity of the protein (45 600 M^{-1} cm^{-1}) calculated according to the method of Gill and von Hippel (*24*).

Determination of TauD Activity under Conditions of Stopped-Flow and Freeze-Quench Experiments. The procedure of Eichhorn et al. (*18*), which utilizes colorimetric quantitation of sulfite by its reaction with Ellman's reagent, was modified slightly for determination of TauD activity at 5 °C and pH 7.6, the reaction conditions employed in the stopped-flow and freeze-quench experiments. To each 1 mL aliquot of air-saturated assay solution containing 50 mM Tris·HCl, pH 7.6, 5 mM taurine, and 5 mM αKG was added 10 *μ*L of a solution containing 50 *μ*M TauD and 10 mM ferrous ammonium sulfate in 10 mM imidazole·HCl, pH 6.9. The reaction was allowed to proceed at 5 °C for times from 30 to 90 s and was then terminated by addition of 300 *μ*L of 0.5 M trichloroacetic acid. Within 30 s of termination, the solution was neutralized with 300 *μ*L of 0.5 M NaOH. Within another 30 s, 100 *μ*L of a 2.5 mM solution of Ellman's reagent in 50 mM Tris·HCl, pH 7.6, was added. After a ∼20 min incubation to allow for reaction of the sulfite and Ellman's reagent, the absorbance at 411 nm (A_{411}) was determined. The quantity of sulfite produced by TauD in each assay solution was determined by comparison of its A_{411} to those of standard samples for which known quantities of added sodium sulfite were reacted with Ellman's reagent.

Titration of TauD with Fe(II) to Determine Maximum Stoichiometry of Binding. Samples of concentrated, pure apo TauD were dialyzed against 50 mM Tris·HCl, pH 7.6, to remove the glycerol from the protein solution. Oxygen was removed from the protein by placing it into a vacuum flask and exchanging the headspace of the flask with argon on a vacuum/gas manifold. After ∼30 cycles of gentle evacuation and refilling with argon over a period of ∼1 h, during which time the protein was gently stirred on ice, and the flask was

sealed and kept at 0 °C overnight to allow for equilibration of the solution and gas phases. In a glovebox (MBraun; Peabody, MA) with a nitrogen atmosphere, buffered, O_2-free solutions of taurine, αKG, and ferrous ammonium sulfate were prepared from dry stocks. Aliquots of the taurine and αKG stock solutions were added to the TauD solution (see legend to Figure 1 for concentrations). The protein solution was centrifuged for 4 min at the maximum speed in an Eppendorf Minispin microcentrifuge and placed in a cuvette, which was then sealed with a rubber septum. The cuvette was removed from the glovebox and this solution was used to "blank" the HP8453 diode array spectrophotometer. An aliquot of the buffered ferrous ammonium sulfate solution was added to the protein solution through the rubber septum. The solution was gently mixed and its absorption spectrum acquired. Additional aliquots were added until the absorbance at 520 nm no longer increased, indicating that saturation had been achieved.

Stopped-Flow Absorption Experiments and Kinetic Simulations. Stopped-flow absorption experiments were carried out at 5 °C in an Applied Photophysics (Surrey, U.K.) SX.18MV apparatus equipped with a diode array detector and housed in the MBraun anoxic chamber. O_2-free stocks of the TauD·Fe(II)·αKG ternary or TauD·Fe(II)·αKG·taurine quaternary complex were prepared as described above for the Fe(II) titration experiment, with the exception that ferrous ammonium sulfate was added to the protein in a single aliquot in the glovebox prior to centrifugation and loading into the stopped-flow apparatus. The TauD complex solution was mixed in the stopped-flow apparatus with an equal volume of either buffer A that had been allowed to reach equilibrium at 0 °C with a gas phase of 1.05 atm O_2 (Figures 3A and 4) or O_2-free buffer A (Figure 3B). In the former experiment, a final O_2 concentration of 1 mM was assumed to result (*25*). Other reactant concentrations are given in the legend to Figure 3. A path length of 0.2 cm and an integration time of 1.28 ms were used. Kinetic simulations were performed with the program KinTekSim (KinTek Corporation; State College, PA).

Preparation of Mössbauer and EPR Samples. The (non-freeze-quenched) samples used to acquire Mössbauer spectra for the TauD·Fe(II) binary and TauD·Fe(II)·αKG·taurine quaternary complexes (Figure 2, spectra A and B) were prepared as described above, with the exception that the iron stock contained ^{57}Fe(II) and was prepared as previously described (*26*) by dissolution of ^{57}Fe(0) in O_2-free 2 N H_2SO_4. Prior to its addition to the protein, the final, acidic ^{57}Fe(II) stock (50 mM Fe(II) in 100 mM remaining H^+) was mixed with 0.5 volume equivalents of O_2-free 1 M Tris·HCl, pH 7.6, to avoid transient acidification of the protein solution. After the samples were fully constituted (see legend to Figure 2 for concentrations), they were transferred to Mössbauer cells, sealed in vials, removed from the glovebox, frozen by immersion of the vials in liquid nitrogen, removed from the vials, and stored in liquid nitrogen.

The apparatus and procedure for preparation of freeze-quenched Mössbauer and EPR samples have been described (*27*). The TauD·^{57}Fe(II)·αKG·taurine complex was prepared in the glovebox as above, loaded into a syringe, and removed from the glovebox. By actuation of the drive motor, this solution was mixed at 5 °C in a volume ratio of 1:2 with O_2-saturated buffer A. In preparation of samples for cryoreduction, glycerol (20% w/v) was present in both protein and O_2 solutions. The resulting reaction solution was passed through an "aging hose" of length appropriate to give the desired reaction time, and the reaction was terminated by injection of the solution into the cold (−150 °C) 2-methylbutane cryosolvent. The total reaction time was calculated as the sum of the known time for transit through the aging hose and the "quench time," the time elapsed between injection of the reaction solution into the cryosolvent and its cooling to a temperature below which no further reaction occurs. For the latter quantity, an estimate of 10 ms was obtained in our earlier work on a different system (*28*) and was assumed in this study.

Mössbauer Spectroscopy. Mössbauer spectra were recorded on spectrometers from WEB research (Edina, MN) operating in the constant acceleration mode in a transmission geometry. Spectra were recorded with the temperature of the sample maintained at 4.2 K. For low-field spectra, the sample was kept inside a SVT-400 dewar from Janis (Wilmington, MA), and a magnetic field of 40 mT was applied parallel to the γ-beam. For high-field spectra, the sample was kept inside a 12SVT dewar (Janis), which houses a superconducting magnet that allows for application of variable magnetic fields between 0 and 8 T parallel to the γ-beam. The isomer shifts quoted are relative to the centroid of the spectrum of a metallic foil of α-Fe at room temperature. Data analysis was performed using the program WMOSS from WEB research.

EPR Spectroscopy. EPR spectra were recorded on an ESP300 spectrometer from Bruker (Billerica, MA) equipped with a ER 041 MR Microwave Bridge and a 4102ST X-band Resonator from Bruker. The temperature was maintained at 77 K by immersion of the sample in liquid nitrogen in a "finger dewar."

Cryoreduction by Low-Temperature γ-Radiolysis. Freeze-quenched 20-ms samples suitable for EPR and Mössbauer spectroscopy were irradiated in the γ-irradiation facility of the Breazeale nuclear reactor at Penn State University using a ^{60}Co-source (activity 26 krad/h). A total dose of ca. 1.4 Mrad was delivered. During the γ-irradiation, the temperature of the samples was maintained at 77 K by immersion in liquid nitrogen.

RESULTS

Determination of Optimum Fe(II)/TauD Ratio and Reactant Concentrations. As a prelude to the kinetic/spectroscopic experiments to address the mechanism of TauD, equilibrium binding measurements similar to those previously reported by Ryle et al. (*19*) were carried out to determine the optimum Fe(II)/TauD stoichiometry. Consistent with the previous work, the visible chromophore of the TauD·Fe(II)·αKG·taurine quaternary complex was seen to develop rapidly (on the time scale of the manual mixing) as Fe(II) was added in the absence of O_2 to a solution containing the enzyme (typically 0.5−1 mM) and its two substrates (5 mM each) (Figure 1). Plots of the background-corrected (protein absorption removed) absorbance at 520 nm (the λ_{max} of the complex) as a function of the concentration of Fe(II) (inset to Figure 1) could be analyzed to give an apparent dissociation constant (K_d) for the complex of 6 ± 4 μM and a maximum complex stoichiometry of 0.87 ± 0.05 Fe(II)/TauD

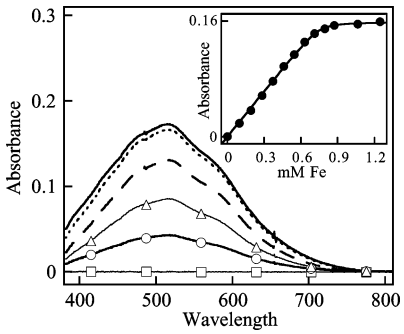

FIGURE 1: Absorption spectra acquired during titration at room temperature of TauD (0.88 mM) with Fe(II) in the absence of O_2 and the presence of 5 mM αKG and 5 mM taurine. The sample prior to the first addition of Fe(II) (containing all other components) was used as spectral reference. The spectra shown correspond to 1.2 mM (solid line), 0.86 mM (dotted line), 0.63 mM (dashed line), 0.41 mM (solid line with triangular symbols), 0.19 mM (solid line with circular symbols), and 0 mM (solid line with square symbols) Fe(II). The points in the inset depict the absorbance at 520 nm (background corrected to the line defined by the absorbances at 318 and 800 nm) as a function of concentration Fe(II). The solid line is a fit of the quadratic equation for binding to the data. The fits from all (6) such titrations gave a mean (± standard deviation) Fe(II)/TauD stoichiometry of 0.87 (± 0.05) and a mean (± standard deviation) dissociation constant of 6 (± 4) μM.

(means ± standard deviations from six trials). Fe(II)/TauD ratios equal to or slightly greater than the mean stoichiometry were selected for the stopped-flow absorption and freeze-quench Mössbauer experiments. Similar titration experiments (not shown) established, in agreement with results reported by Ryle et al. (*19*), that an αKG concentration of 5 mM is effectively saturating.

Changes at the Fe(II) Site upon Substrate Binding Monitored by Mössbauer Spectroscopy. Also as a prelude to the mechanistic experiments, changes at the Fe(II) center upon conversion of the TauD·Fe(II) binary complex to the TauD·Fe(II)·αKG·taurine quaternary complex were monitored by Mössbauer spectroscopy. The spectrum of the binary complex, recorded at 4.2 K in a 40-mT magnetic field applied parallel to the γ-beam, is shown in Figure 2A. It can be simulated as a broad quadrupole doublet with parameters (isomer shift, δ, of 1.27 ± 0.05 mm/s; quadrupole splitting, ΔE_Q, of 3.06 ± 0.05 mm/s) typical of high-spin Fe(II). Upon addition of αKG and taurine (Figure 2, spectrum B), the Mössbauer parameters change significantly ($\delta = 1.16 \pm 0.05$ mm/s, $\Delta E_Q = 2.76 \pm 0.05$ mm/s). The reduction in isomer shift upon binding of the substrates has been shown to occur in other mononuclear non-heme-Fe(II) enzymes (*29*, *30*) and is consistent with the conversion of a six-coordinate Fe(II) site to a five-coordinate, square-pyramidal site.

Stopped-Flow Absorption Evidence for Two Intermediates in the TauD Reaction. The time-dependent absorption spectra acquired after initiation of the hydroxylation reaction at 5 °C by mixing of the TauD·Fe(II)·αKG·taurine quaternary complex with O_2-saturated buffer provide clear evidence for the accumulation of two distinct intermediate states prior to the regeneration of the initial quaternary complex following consumption of O_2. To illustrate this conclusion, the essentially invariant spectra from a control experiment in which the quaternary complex was mixed with *O_2-free* buffer (Figure 3B) have been subtracted from the experimental, time-dependent spectra of the complete reaction (Figure 3A).

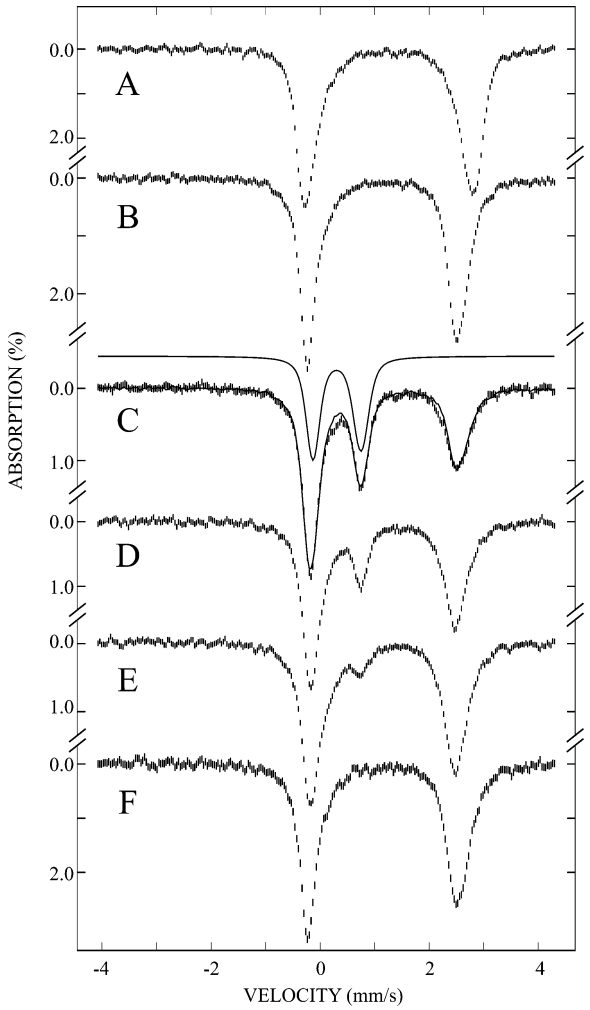

FIGURE 2: Mössbauer spectra of TauD samples recorded at 4.2 K in a 40-mT magnetic field applied parallel to the γ-beam. A and B are spectra of the binary TauD·Fe(II) complex and the quaternary TauD·Fe(II)·αKG·taurine complex, respectively. These samples contained 2.25 mM TauD, 1.09 mM ^{57}Fe(II) and either (A) 0 or (B) 5 mM αKG and taurine. C through F are spectra of freeze-quenched samples from the reaction of the quaternary TauD·Fe(II)·αKG·taurine complex with O_2. The concentrations after mixing were 1.5 mM TauD, 1.5 mM ^{57}Fe(II), 5 mM αKG, 5 mM taurine and 1.3 mM O_2. The reaction times were (C) 20 ms, (D) 80 ms, (E) 200 ms, and (F) 5 min. The solid line above spectrum C is a theoretical simulation, generated by using the parameters quoted in the text, of the spectrum of the intermediate. The simulated spectrum has been normalized to 46% of the area of spectrum C. The solid line overlaid with spectrum C is the summation of the simulated spectrum at this percentage with the spectrum of the quaternary TauD·Fe(II)·αKG·taurine complex (50% of B).

The control establishes that the changes that are observed in the complete reaction are associated with reaction of the complex with O_2, and the subtraction removes absorption from the protein (including the reactant complex) and contaminants so as to reveal these changes more clearly. An additional control experiment was conducted to confirm that, as reported by Ryle et al. (*19*), absorbance changes are smaller and are observed only on a much longer time scale when the ternary TauD·Fe(II)·αKG complex (i.e., with taurine omitted) is mixed with O_2 (Figure 4B). The first intermediate state in the complete reaction is characterized by an absorption feature centered at 318 nm (Figure 3C, solid trace). It develops to its maximum extent within the first 20−25 ms and then decays within a reaction time of ∼ 600

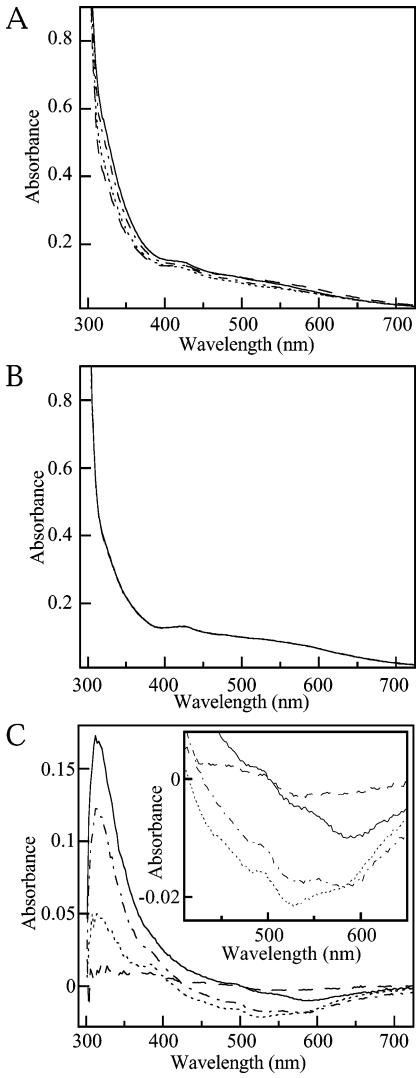

FIGURE 3: UV−visible absorption spectra acquired after equal-volume mixing at 5 °C of a solution of 2.4 mM TauD, 2.2 mM Fe(II), 10 mM αKG, and 10 mM taurine in 50 mM Tris·HCl, pH 7.6, with (A) O_2-saturated buffer or (B) O_2-free buffer. Panel C shows the subtraction of the spectra in B from those in A. The spectra were recorded 20 ms (solid lines), 68 ms (dot−dashed lines), 210 ms (dotted lines), and 10 s (dashed lines) after mixing.

ms (Figure 4A, circular points). The difference spectrum corresponding to the time of maximal accumulation of the first intermediate state exhibits, in addition to the positive feature at 318 nm, a less intense negative feature at lower energy attributable to loss of the charge-transfer band of the reactant complex (Figure 3C, solid trace). The minimum of this difference spectrum is, however, red-shifted by approximately 65 nm from the peak of the reactant complex that has decayed (inset to Figure 3C). This shift is attributable to (i) significant absorption by the first intermediate in the region of the λ_{max} of the starting complex and (ii) the more precipitous "trailing off" toward lower energy of the intermediate's spectrum in comparison with that of the starting complex. Indeed, the intermediate is approximately isosbestic with the starting complex at its λ_{max} of 520 nm, and, consequently, the kinetic trace at this wavelength exhibits a lag phase during the accumulation of the intermediate (Figure 4A, squares). This coincidence may (in addition to differences in the reaction conditions employed) explain why evidence for the intermediate was not previously noted. As decay of the first intermediate proceeds, the difference spectrum comes to reflect more closely the negative feature at 520 nm attributable to loss of the starting quaternary complex (Figure 3C, dotted trace in main figure and inset). This observation indicates that the second intermediate state has less absorption than the first in this spectral region. Finally, the weakly absorbing second intermediate state decays as the starting quaternary complex is regenerated and its 520 nm absorption returns, resulting in a nearly featureless difference spectrum (Figure 3C, dashed trace).

Trapping of a Novel Fe Intermediate and Characterization by Mössbauer Spectroscopy. The nature of the intermediate states was probed by rapid freeze-quench Mössbauer spectroscopy. The 4.2-K/40-mT spectrum of a sample that was rapidly frozen ("freeze-quenched") after a reaction time of 20 ms, near the time of maximum absorbance at 318 nm in the stopped-flow experiments, exhibits a contribution from the high-spin Fe(II) site of the reactant complex and an additional prominent peak at 0.75 mm/s (Figure 2, spectrum C). The deconvolution of this spectrum (solid line plotted over spectrum C in Figure 2) reveals that it is composed of 50 ± 3% of the spectrum of the quaternary complex (spectrum B) and 46 ± 3% of a quadrupole doublet with $\delta = 0.31 \pm 0.03$ mm/s and $\Delta E_Q = 0.88 \pm 0.03$ mm/s (solid line plotted above spectrum C). Spectra of samples in which the reaction was quenched after 80 ms, 200 ms, and 5 min (Figure 2, spectra D, E, and F) can be analyzed as superpositions of the contributions from high-spin Fe(II) and the $\delta = 0.31$ species.[2] They reveal that the absorption of the new species decreases with increasing time (27 ± 3% after 80 ms, 13 ± 3% after 200 ms, and zero after 5 min). Thus, the Mössbauer spectra unambiguously demonstrate the accumulation of a novel Fe intermediate in the reaction of the TauD·Fe(II)·αKG·taurine complex with O_2.

Further insight into the electronic structure of the novel intermediate was obtained by determination of its Mössbauer spectrum in a magnetic field of 8 T applied parallel to the γ-beam. The spectrum of the intermediate (Figure 5, spectrum B) was obtained by subtracting the experimental spectrum of the reactant complex (solid line in Figure 5, spectrum A) from that of the 20-ms freeze-quenched sample (hatched data points in Figure 5, spectrum A), which contains the maximum concentration of the intermediate. The spectrum of the reactant complex was scaled to an intensity of 50% (its contribution to the spectrum of the 20 ms sample) prior to this subtraction. The spectrum of the intermediate thus obtained provides detailed insight into the nature of the electronic ground state of the intermediate. The fact that the intermediate gives rise to a quadrupole doublet in a weak (40 mT) magnetic field but displays hyperfine interactions in a strong externally applied field is typical of species with integer-spin electronic states. Importantly, the 8-T spectrum

[2] Although the vast majority of intensity that is not associated with the $\delta = 0.31$ mm/s intermediate is, through the entire course of the reaction, attributable to high-spin Fe(II) species, the spectral contribution attributable specifically to the high-spin Fe(II) of the reactant complex changes slightly as a function of reaction time. This observation suggests the presence of varying quantities of one or more additional high-spin Fe(II) species with Mössbauer parameters that are slightly different from those of the reactant complex. The Fe(II) species are not resolved due to their large line-widths and the similarity of their parameters.

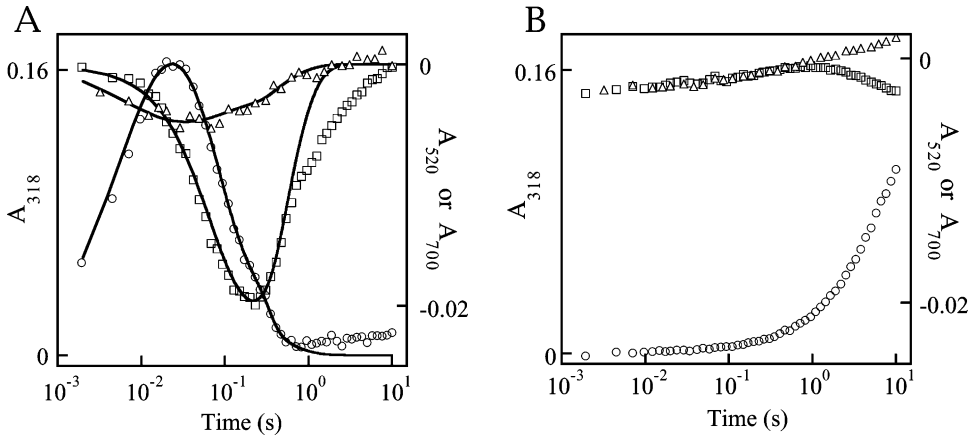

FIGURE 4: Kinetic traces from (A) the reaction of Figure 3A and (B) the reaction of the ternary TauD·Fe(II)·aKG complex (in the absence of taurine) with O_2-saturated buffer under the same conditions. The symbols depict the experimental absorbances at 318 nm (circular points, left axis), 520 nm (square points, right axis), and 700 nm (triangular points, right axis). The solid lines in A are simulations of the kinetic data according to the parameters summarized in Scheme 2 and the text.

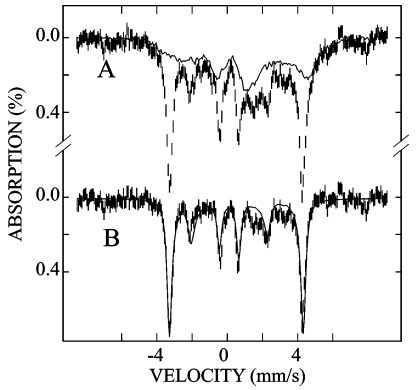

FIGURE 5: Mössbauer spectra of TauD samples recorded at 4.2 K in an 8-T magnetic field applied parallel to the γ-beam. The spectrum of the 20-ms sample is shown in A. Overlaid as a solid line is the experimental 4.2-K/8-T spectrum of the quaternary complex, scaled to 50% of the total absorption of the spectrum of the 20-ms sample. The reference spectrum for the TauD intermediate is shown in B. It is obtained by removing 50% of the spectrum of the quaternary complex from the spectrum of the 20-ms sample. The solid line overlaid with the experimental data in B is a theoretical simulation using the parameters quoted in Table 1.

is a sharp, six-line spectrum with peak separations that reflect an effective magnetic field of ca. 24 T at the ^{57}Fe nucleus. The effective magnetic field is a consequence of an internal magnetic field of ca. 32 T oriented antiparallel to the externally applied 8-T field. The internal magnetic field is given by the expression $\langle \mathbf{S} \rangle \cdot \mathbf{A}/g_N\beta_N$, in which $\langle \mathbf{S} \rangle$ is the expectation value of the electronic spin and $\mathbf{A}/g_N\beta_N$ is the hyperfine tensor for the ^{57}Fe nucleus. $\mathbf{A}/g_N\beta_N$ is dominated by the Fermi contact term, which yields an isotropic value of ca. -22 T. From the magnitude of the internal magnetic field, $B_{int} = 32$ T, we estimate $\langle \mathbf{S} \rangle$ as 1.5 at 8 T. This spin expectation value unambiguously requires that the intermediate have an electronic ground state with $S \geq 2$. The reasonable assumption that the TauD intermediate is mononuclear and the absence of an EPR signal in the $g = 4.3$ region (vide infra) imply that the intermediate has $S = 2$.

The fact that the TauD intermediate has a low isomer shift (0.31 mm/s) and a $S = 2$ ground state, together with the fact that its cryoreduction yields a high-spin Fe(III) species (vide infra), provides strong evidence for a high-spin Fe(IV) assignment. In particular, its isomer shift and quadrupole splitting parameters are very similar to those observed for the high-spin Fe(IV) site of intermediate **X** from ribonucleotide reductase (*31*) (see Table 1 for comparison), suggesting that these two Fe(IV) sites may be similar. We have therefore simulated the 8-T spectrum of the TauD intermediate using the known intrinsic $\mathbf{A}/g_N\beta_N$ tensor of intermediate **X**, and adjusting D and E/D of the $S = 2$ ground state (note that the intrinsic ZFS parameters of the Fe(IV) site of **X** are not known, since **X** has an $S = 1/2$ ground state). Values of $D \approx +15$ cm^{-1} and $E/D \approx 0$ together with $\mathbf{A}/g_N\beta_N = (-20, -20, -15)$ T yield good agreement with the experimental spectrum (solid line in Figure 5, spectrum B). Importantly, simulations show that the width of the outer lines is sensitive to anisotropies of the internal magnetic field within the x−y plane. For $D > 0$ and $E/D = 0$, $\langle \mathbf{S_x} \rangle = \langle \mathbf{S_y} \rangle$, and with $\mathbf{A_{xx}}/g_N\beta_N = \mathbf{A_{yy}}/g_N\beta_N$, isotropic internal fields in the x−y plane are obtained, which reproduce the sharpness of the outer lines well. It should be emphasized that the value of D required for optimal simulation of the experimental spectrum strongly depends on the choice of $\mathbf{A}/g_N\beta_N$. In addition, for $D > 0$ and $E/D \approx 0$, the state lowest in energy has a spin expectation value very close to zero in small magnetic fields and thus gives rise to a quadrupole doublet, as is observed experimentally in the 40-mT spectrum. A precise determination of the complete set of spin Hamiltonian parameters by measurement of Mössbauer spectra in varying externally applied fields and temperatures is in progress and will be reported later.

Cryoreduction of the Novel Fe Intermediate to an Fe(III) Complex. The Mössbauer spectra unambiguously demonstrate that the novel intermediate is paramagnetic and has an integer-spin ground-state of $S \geq 2$. As noted above and elaborated in the Discussion, these properties and its Mössbauer parameters strongly suggest that the Fe center of the intermediate is best described as high-spin Fe(IV). To further corroborate this assignment, we sought to test the prediction that one-electron reduction of the intermediate should produce a high-spin Fe(III) complex. To achieve reduction, we employed γ-radiolysis at low temperature (cryoreduction). In this technique, a glycerol-containing sample is exposed to high-energy radiation (e.g., from a ^{60}Co source), while the sample is immersed in liquid nitrogen. This procedure generates mobile electrons, which can reduce transition metal

Table 1: Comparison of the Intrinsic Mössbauer Parameters of the High-Spin Fe(IV) Sites in the TauD Intermediate and Intermediate **X** from Ribonucleotide Reductase

species	δ [mm/s]	ΔE_Q [mm/s]	η	$A/g_N\beta_N$ [T][a]	D [cm^{-1}][b]	E/D[b]	ref
TauD intermediate	0.31	−0.88	0[c]	(−20,−20, −15)[c]	≈+15	≈0	this work
Fe(IV) site of **X**	0.26	−0.6	2.7	(−20,−20, −15)	nd[d]	nd[d]	*31*

[a] Given with respect to the spin of the Fe(IV) site, $S = 2$. [b] $S = 2$ was assumed for the simulation. [c] Parameter fixed during simulation. [d] Not determined due to the $S = 1/2$ ground state of intermediate **X**.

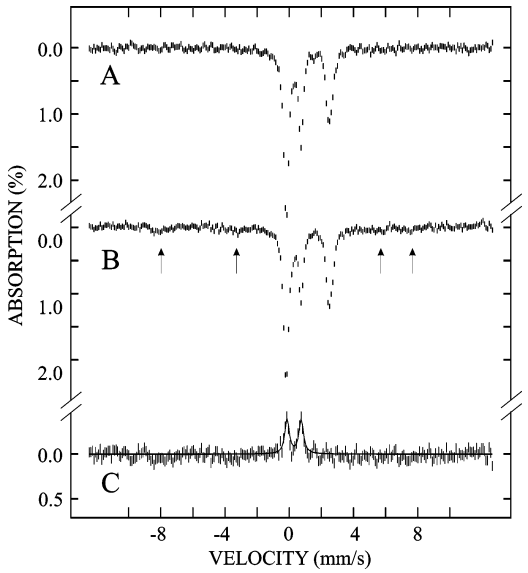

FIGURE 6: 4.2-K/40-mT Mössbauer spectra of a 20-ms sample recorded (A) before and (B) after cryoreduction (as described in the text). Spectrum C is the difference spectrum B − A, and the solid line in C is a theoretical simulation of 13% of the TauD intermediate, which is converted to the new magnetic sub-spectrum (indicated by arrows in B) by cryoreduction.

ions and clusters in metalloproteins (e.g., see ref *32* and references therein). Importantly, the geometry of the metal center is retained during the procedure, because the sample is kept at low temperature (77 K). This technique has been used, for example, to reduce the formally Fe(IV/IV) cluster ***Q*** from methane monooxygenase by one electron to an Fe(III/IV) species (*33*). By analogy, we expected that the high-spin Fe(IV) site of the TauD intermediate could be cryoreduced to a high-spin Fe(III) site.

The Mössbauer spectrum of a glycerol-containing sample in which the quaternary TauD·Fe(II)·αKG·taurine complex was reacted with O_2 for 20 ms prior to freeze-quenching (Figure 6, spectrum A) is essentially identical to the spectrum shown in Figure 2, spectrum C, and is explained as a superposition of spectral contributions from the novel intermediate (45%) and reactant complex (55%). After γ-irradiation of this sample at 77 K with a total dose of 1.4 Mrad (Figure 6, spectrum B), the two quadrupole doublets arising from the quaternary complex and the intermediate are still visible, but a broad, magnetically split component (indicated by arrows) is also detectable. The effect of the γ-irradiation is best represented by the difference spectrum of the experimental spectra taken before and after the procedure (Figure 6, spectrum C). In this representation, the spectral features of the species generated by cryoreduction point downward, and the features of the species that are converted by the procedure point upward. The intensity of the doublet associated with the intermediate is diminished by 13% (from 45% of the total intensity before reduction to 32% after reduction) by the procedure. Thus, the cryoreduction yield under these conditions is ca. 30% (13/45). Importantly, the contribution from the quaternary complex (55% of the total intensity) is unchanged, implying that only the Fe site of the intermediate is susceptible to cryoreduction. The decrease in the absorption of the quadrupole doublet associated with the intermediate is accompanied by the appearance of a broad, magnetically split component extending from −8 mm/s to + 8 mm/s. Although these features are weak and not very well resolved, they are reminiscent of a high-spin Fe(III) center in the slow relaxation limit, as is expected for the one-electron reduced state of the high-spin Fe(IV)-containing intermediate.

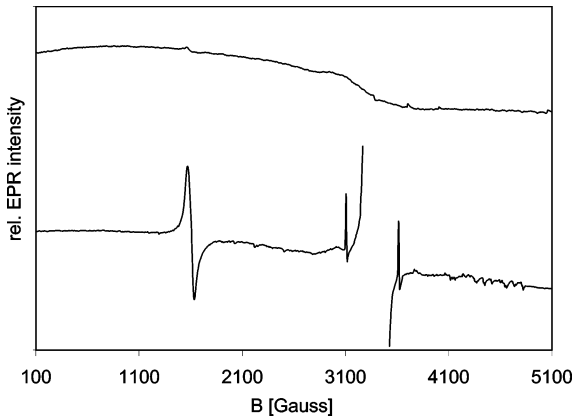

FIGURE 7: 77-K X-band EPR spectra of a 20-ms sample recorded before (top) and after (bottom) cryoreduction. Experimental parameters were: frequency, 9.51 GHz; power, 2 mW; modulation amplitude, 10 G; modulation frequency, 100 kHz.

To obtain further evidence that the cryoreduced species contains a high-spin Fe(III) site, we monitored the effect of γ-irradiation also by EPR spectroscopy. No EPR signals are detected in the spectrum recorded before cryoreduction (Figure 7 top), as is expected for a sample containing integer spin Fe-centers (both the intermediate and the quaternary complex have an $S = 2$ ground state). After irradiation, several EPR-active species are observed (Figure 7 bottom). In addition to an intense signal at $g = 2$ originating from organic radicals, there is a pronounced, quasi-isotropic signal at $g = 4.2$, which is typical of high-spin Fe(III) sites in nearly rhombic environments. Taken together, the Mössbauer and EPR data provide strong evidence for the conversion of the novel intermediate to a high-spin Fe(III) species by cryoreduction. This demonstration is, in turn, strong evidence for assignment of the formal oxidation state of the intermediate as +IV.

The Nature of the Second Intermediate State and Its Conversion to the Reactant Complex. Decay of the Mössbauer signature of the first intermediate species is associated with the return of quadrupole doublet components attributable to Fe(II) species. This observation and the above conclusion that the second intermediate state absorbs weakly suggest

Scheme 2: Kinetic Mechanism Used to Simulate the Stopped-Flow Data and the Kinetics of the First Intermediate Determined by Mössbauer[a]

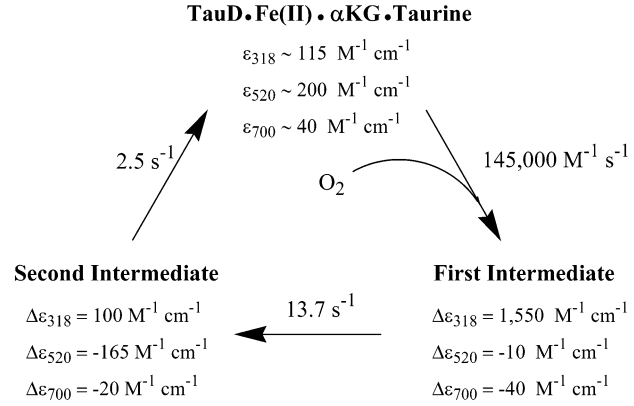

[a] Each $\Delta\epsilon$ parameter represents the difference in the molar absorptivity of the intermediate state at the wavelength indicated by the subscript from the corresponding value of the reactant complex.

that it is a TauD·Fe(II)·product complex, the TauD·Fe(II) binary complex, or a mixture thereof. Ryle et al. (*19*) previously showed that binding of αKG to the binary TauD·Fe(II) complex to generate the visible chromophore is relatively slow and that subsequent binding of taurine is fast (>140 s^{-1}). They further showed that the kinetics of αKG binding are independent of αKG concentration. This result suggests that a unimolecular step (e.g., a protein conformational change or dissociation of an Fe ligand) is rate-limiting for binding of αKG. The apparent first-order rate constant that they reported for the binding reaction at 4 °C (4.4 ± 2.8 s^{-1}) is not significantly different from the rate constant of 2.5 s^{-1} (at 5 °C) that we have deduced for conversion of the second intermediate state into the reactant quaternary complex (see below). Thus, it is likely that the single observed step in which the second intermediate is converted into the quaternary complex is composed of three elementary steps, the rate-limiting unimolecular step followed by rapid binding of αKG and taurine.

Simulation of the Stopped-Flow Kinetic Data and Prediction of the Steady-State Turnover Rate. The kinetic traces from three diagnostic wavelengths: 318 nm (circles, lefthand axis), where the first intermediate dominates; 520 nm (squares, righthand axis), where the reactant complex and the first intermediate both absorb; and 700 nm (triangles, righthand axis), where the reactant complex and the second intermediate state contribute (see below), are shown in Figure 4A. These traces have initial and final absorbance values of zero because, as in Figure 3C, the absorption from the reactant complex has been removed by subtraction. The traces can be simulated according to Scheme 2. The parameters of the simulations are the concentrations of the quaternary complex and O_2, the rate constants for the three steps of the reaction sequence, and the changes in molar absorptivity ($\Delta\epsilon$) from those of the reactant complex for the two intermediates at the three wavelengths. These parameters are summarized in Scheme 2, along with estimates from the titration experiments of the molar absorptivities of the reactant complex at the three wavelengths. The quantities of the first intermediate determined in the freeze-quench Mössbauer experiments provide crucial constraints for this simulation. With rate constants consistent with the stopped-flow data, the simulation overpredicts the quantities of the intermediate if it is assumed that the concentration of the starting quaternary complex is equal to the known concentration of the limiting constituent (Fe(II) or TauD, depending on whether the Fe(II)/TauD ratio was less than or greater than the complex stoichiometry of 0.9 determined in the titration experiments). This observation suggests that a fraction of the starting complex either is unreactive toward O_2 or reacts with markedly different (slower) kinetics. Heterogeneity in reactivity is commonly observed in "single-turnover" experiments with enzymes and seems to be observed almost invariably in Fe-dependent oxidases and oxygenases (see, for example, references (*28*, *34*)). Best agreement between the simulation and data is obtained when it is assumed that the concentration of the reactive complex is 0.72 times the expected concentration.[3] With this assumption and the parameters given in Scheme 2, the stopped-flow kinetic traces can be simulated well (compare solid lines and data points in Figure 4A; see below for discussion of the imperfect agreement between the A_{520} traces at long reaction time), and the predicted concentrations of the first intermediate (solid line in Figure 8) match almost precisely with those determined by Mössbauer (data points in Figure 8).

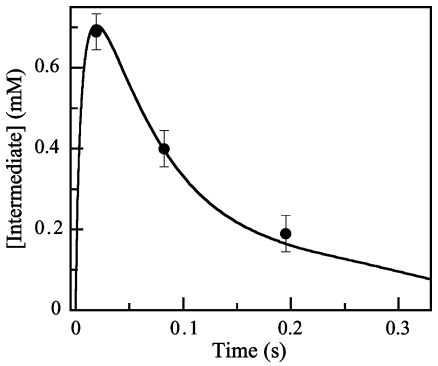

FIGURE 8: Comparison of the concentrations of the first intermediate determined by analysis of spectra C−F of Figure 2 (data points) with those predicted by Scheme 2 (solid line).

The steady-state turnover number predicted by Scheme 2 (with the O_2 concentration expected of an air-saturated solution, the condition under which our activity assays have been carried out) is 1.3 s^{-1}. Here, it has again been assumed that 0.72 of the enzyme is reactive. The fact that the measured value of 1.3 ± 0.2 s^{-1} (mean ± standard deviation for four independent trials) agrees well with the predicted value establishes that all three observed steps are kinetically competent to be constituents of the hydroxylation pathway.

DISCUSSION

Kinetic Description of the TauD Reaction. The demonstration that Scheme 2 can satisfactorily account for the experimental kinetic traces at three diagnostic wavelengths,

[3] As an alternative to heterogeneity in the reactant, the assumption of reversibility in formation of the first intermediate can correct the overprediction of the quantities of the first intermediate as a function of time. This reversibility would have important implications for the identity of the intermediate, and could be demonstrated by explicit variation of the concentrations of the reactants (the quaternary complex and O_2). In the absence of direct demonstration of reversibility, we consider reactant heterogeneity to be the simplest and most probable explanation.

the kinetics of the first intermediate determined independently in the freeze-quench Mössbauer experiments, and the steady-state turnover number indicates that it accurately reflects important features of the TauD catalytic cycle. However, it clearly also contains some simplifications and untested assumptions. First, it presumes the bimolecular nature of the step in which the first intermediate is formed, and this kinetic characteristic has not been verified by explicit variation of reactant concentrations. Second, it considers all three steps as irreversible. The likelihood that this assumption is correct is dependent on the placements of the intermediate states in the TauD cycle. Clearly, decarboxylation of αKG and O−O bond cleavage are expected to be irreversible, but earlier steps may not be. Perhaps most importantly, the scheme takes no account of the fact that significant concentrations of the products, succinate, 1-hydroxytaurine (or its breakdown products) and CO_2, are produced through the course of the reaction. The time-dependent accumulation of these products could complicate the kinetics of recovery of the reactant complex in the last phase of the reaction. This complication could rationalize the only significant discrepancy between the simulations and the data, the ∼1−10 s regime of the A_{520}-versus-time trace. As seen in Figure 4A, a very slow phase of recovery of the 520 nm absorption characteristic of the reactant complex is not predicted by Scheme 2. Among all the kinetic phases for all three wavelengths, it is the recovery phase of A_{520} that should, according to Scheme 2, be most diagnostic of the conversion of the second intermediate into the reactant quaternary complex. Therefore, the disagreement between the simulation and data probably arises from an oversimplification relative to this step that is inherent in Scheme 2, and the most likely culprit is the unaccounted-for accumulation of products. The ability of Scheme 2 to accurately predict the steady-state rate provides support for this attribution. The slow phase of recovery of A_{520} is much too slow (from approximation of the 1−10 s portion of the A_{520} kinetic trace as a first-order process, a rate constant of 0.4 s^{-1} is estimated) to be part of a catalytic cycle operating at 1.3 s^{-1}, and, of course, this turnover number has been determined under initial velocity conditions (i.e., in the absence of products).

Identity of the Novel TauD Fe Intermediate. The most intriguing issue raised by the above results is the identity of the novel first intermediate. Two arguments provide strong evidence that the novel intermediate contains a formally high-spin Fe(IV) center. (i) The Mössbauer spectra show that the intermediate has an integer spin ground state with $S \geq 2$. Since TauD is a mononuclear Fe enzyme, we conclude that it has an $S = 2$ ground state. (ii) Cryoreduction of the TauD intermediate is accompanied by the formation of a high-spin Fe(III) species. Therefore, the intermediate must have a formal oxidation state greater than +III, i.e., +IV.

The isomer shift of the novel intermediate ($\delta = 0.31$ mm/s) is, however, unusually large for an Fe(IV) species. The majority of known Fe(IV) species, including the many heme Fe(IV)═O^{2-} intermediates (see ref *35* and references therein) and several inorganic heme and non-heme models (e.g., refs *36*−*39*) that have been characterized have isomer shifts less than 0.14 mm/s. All of these species contain *low-spin* ($S = 1$) Fe(IV) sites, and their electronic structures may be significantly different from that of the proposed high-spin ($S = 2$) Fe(IV) site of the TauD intermediate. To our knowledge, mononuclear, high-spin Fe(IV) species are unknown to date. High-spin Fe(IV) sites have, however, been demonstrated or proposed in several protein and inorganic dinuclear Fe complexes. In one model system, a high-spin Fe(IV)═O^{2-} site has been proposed to form by isomerization of an Fe(III)−$(O^{2-})_2$−Fe(IV) species to a putative Fe(III)-O^{2-}-Fe(IV)═O^{2-} unit (*40*). The Fe(IV) site in this complex has an isomer shift of 0.10 mm/s, toward the upper end of the range characterizing the low-spin Fe(IV) complexes but still considerably less than that of the TauD intermediate. Significantly larger isomer shifts have been observed for the high-spin Fe(IV) site of the formally Fe(IV)Fe(III) complex **X** in ribonucleotide reductase protein R2 ($\delta = 0.26$ mm/s (*31*)) and the two (putatively high-spin) Fe(IV) sites of the formally Fe(IV)Fe(IV) complex **Q** in methane monooxygenase (δ between 0.14 and 0.21 mm/s for its two sites (*34*, *41*)). These two protein diiron complexes (especially the former) provide encouragement that an isomer shift as high as 0.31 mm/s may be possible for a high-spin mononuclear Fe(IV) species. One factor that could contribute to the unusually high isomer shift of the TauD intermediate is electron donation by the ligands, which would confer Fe(III) character to the high-valent site. This notion has previously been advanced to explain the observation that the isomer shifts of the Fe(IV) sites in the aforementioned protein-bound diiron intermediates are invariably greater than those of the most directly comparable inorganic models for them. For example, the formally Fe(IV) site in the protein intermediate, cluster **X** from ribonucleotide reductase, has an isomer shift (0.26 mm/s) 0.16 mm/s greater than the Fe(IV) site in the putative Fe(III)−O^{2-}−Fe(IV)═O^{2-} model complex with which it shares the same number of valence electrons. The Fe(IV) site of an Fe(III)Fe(IV) model with exclusively carboxylate coordination (as opposed to the pyridine and amine coordination of the first model complex) has a significantly larger isomer shift (0.19 mm/s) (*42*), suggesting that one simple factor that can influence the capacity of the coordination sphere to confer partial Fe(III) character and thereby increase isomer shift is the chemical nature or charge of the ligands. Perhaps the Fe ligands of the TauD intermediate are particularly well-suited to partially absorb the iron high-valency by strong electron donation.

In the following, we discuss **I**−**IV** of Scheme 1 as candidate structures for the novel intermediate. Of these, we strongly disfavor structure **IV**, which could be produced by abstraction of a hydrogen atom from C-1 of taurine by an Fe(IV)═O^{2-} complex, for the following two reasons. First, we consider it extremely unlikely that a state containing a substrate radical would accumulate, i.e., be stable relative to its precursor, and second, it seems unlikely that the Fe site of **IV** would have sufficient Fe(IV) character to be consistent with the low isomer shift of 0.31 mm/s.

Each of the remaining structures, **I**, **II**, and **III**, can be depicted as a resonance hybrid with formally Fe(IV) and Fe(III) contributors, as is suggested by the spectroscopic data on the intermediate. Unfortunately, none of these structures has direct precedent among known inorganic or protein complexes.

Of the three, we consider **I**, in which the O_2-moiety is bound end-on to the Fe center, to be the least likely candidate. Formation of a species with significant Fe(IV) character by a simple two-electron oxidative addition of O_2 to an Fe(II)

precursor is, to our knowledge, unprecedented. In fact, computational studies by Solomon and co-workers suggest that this initial Fe(II)-O_2 adduct would best be described as a high-spin Fe(III) ($S = 5/2$) antiferromagnetically coupled to a superoxide radical anion ($S = 1/2$) to yield an $S = 2$ ground state (*43*). The isomer shift of the TauD intermediate is significantly lower that of similar high-spin Fe(III) sites (e.g., the Fe(III) form of tyrosine hydroxylase (*44*) exhibits an isomer shift of 0.56 mm/s). However, in the absence of more direct experimental precedent, we do not feel justified to exclude structure **I** from consideration.

The second possible structure of the TauD intermediate is the bicyclic peroxyhemiketal complex (**II** in Scheme 1) resulting from attack of the uncoordinated oxygen of species **I** on the ketone carbonyl of αKG. Conceivable resonance formulations for such a species would include both Fe(IV)-peroxo and Fe(III)-superoxo contributors. It is not obligatory that an intermediate of this structure occur in the conversion of the initial Fe(II)-O_2 adduct to the presumptive Fe(IV)═O^{2-} hydroxylating species: the attack of the uncoordinated oxygen on the αKG carbonyl and decarboxylation could also be concerted rather than sequential, as is shown in Scheme 1. However, precedent for this structural motif is found in the coordination chemistry of rhodium (*45*, *46*), iridium (*46*, *47*), and cobalt (*46*). In particular, Rh and Ir complexes, in which the metal is in the +III oxidation state and is facially coordinated by the peroxide and a bidentate quinone hemiketal anion, have been structurally characterized (*45*, *47*). Analogous Fe complexes are, to our knowledge, not known, but they have been proposed as intermediates in the reaction cycles of several mononuclear non-heme-Fe enzymes (*1*, *17*, *20*).

The third possibility is that the intermediate is an Fe(IV)═O^{2-} species with associated resonance formulations (**III** in Scheme 1). As previously noted, many such species have been characterized in heme proteins (see ref *35* and references therein), but they all have low-spin ($S = 1$) electronic ground states. The only high-spin Fe(IV)═O^{2-} species reported to date is the putative dinuclear Fe(III)−O^{2-}−Fe(IV)═O^{2-} species (*40*).

In conclusion, we have obtained kinetic and spectroscopic evidence for an intermediate in the reaction of taurine/αKG dioxygenase, TauD, with dioxygen. Importantly, it is the first report of an oxidized intermediate for any of the Fe(II)/αKG-dependent enzymes. This intermediate is kinetically competent to be on the taurine hydroxylation pathway. We have demonstrated by Mössbauer spectroscopy that this species contains a formally high-spin Fe(IV) site. Ongoing spectroscopic characterization of the intermediate should allow for definitive assignment of its structure, while kinetic studies to test for temporal correlation between its formation or decay and transformation of the substrates (or their chemical or isotopic derivatives) should permit placement of the species within the TauD catalytic cycle. The study thus sets the stage for a dissection of the TauD reaction that should provide unprecedented insight into the mechanism of oxygen activation by the αKG-dependent dioxygenases.

ACKNOWLEDGMENT

We thank Candace C. Davison of the Breazeale Nuclear Reactor Facility for her assistance with the γ-irradiation experiments.

REFERENCES

1. Que, L., Jr., and Ho, R. Y. N. (1996) *Chem. Rev. 96*, 2607−2624.
2. Ryle, M. J., and Hausinger, R. P. (2002) *Curr. Opin. Chem. Biol. 6*, 193−201.
3. Prescott, A. G., and Lloyd, M. D. (2000) *Nat. Prod. Rep. 17*, 367−383.
4. Baldwin, J. E., and Bradley, M. (1990) *Chem. Rev. 90*, 1079−1088.
5. Baldwin, J. E., Adlington, R. M., Crouch, N. P., Schofield, C. J., Turner, N. J., and Aplin, R. T. (1991) *Tetrahedron 47*, 9881−9900.
6. Choroba, O. W., Williams, D. H., and Spencer, J. B. (2000) *J. Am. Chem. Soc. 122*, 5389−5390.
7. Ivan, M., Kondo, K., Yang, H., Kim, W., Valiando, J., Ohh, M., Salic, A., Asara, J. M., Lane, W. S., and Kaelin, W. G., Jr. (2001) *Science 292*, 464−468.
8. Jaakkola, P., Mole, D. R., Tian, Y.-M., Wilson, M. I., Gielbert, J., Gaskell, S. J., von Kriegsheim, A., Hebestreit, H. F., Mukherji, M., Schofield, C. J., Maxwell, P. H., Pugh, C. W., and Ratcliffe, P. J. (2001) *Science 292*, 468−472.
9. Epstein, A. C. R., Gleadle, J. M., McNeill, L. A., Hewitson, K. S., O'Rourke, J., Mole, D. R., Mukherji, M., Metzen, E., Wilson, M. I., Dhanda, A., Tian, Y.-M., Masson, N., Hamilton, D. L., Jaakkola, P., Barstead, R., Hodgkin, J., Maxwell, P. H., Pugh, C. W., Schofield, C. J., and Ratcliffe, P. J. (2001) *Cell 107*, 43−54.
10. Bruick, R. K., and McKnight, S. L. (2001) *Science 294*, 1337−1340.
11. Trewick, S. C., Henshaw, T. F., Hausinger, R. P., Lindahl, T., and Sedgwick, B. (2002) *Nature 419*, 174−178.
12. Duncan, T., Trewick, S. C., Koivisto, P., Bates, P. A., Lindahl, T., and Sedgwick, B. (2002) *Proc. Natl. Acad. Sci. U.S.A. 99*, 16660−16665.
13. Kivirikko, K. I. (1993) *Ann. Med. 25*, 113−126.
14. Kuutti-Savolainen, E. R., Risteli, J., Miettinen, T. A., and Kivirikko, K. I. (1979) *Eur. J. Clin. Invest. 9*, 89−95.
15. Hocart, C. H., Halpern, B., Hick, L. A., Wong, C. O., Hammond, J. W., and Wilcken, B. (1983) *J. Chromatogr. 275*, 237−243.
16. Verhoeven, N. M., Wanders, R. J. A., Poll-The, B. T., Saudubray, J. M., and Jakobs, C. (1998) *J. Inherited Metab. Dis. 21*, 697−728.
17. Solomon, E. I., Brunold, T. C., Davis, M. I., Kemsley, J. N., Lee, S.-K., Lehnert, N., Neese, F., Skulan, A. J., Yang, Y.-S., and Zhou, J. (2000) *Chem. Rev. 100*, 235−349.
18. Eichhorn, E., Van Der Ploeg, J. R., Kertesz, M. A., and Leisinger, T. (1997) *J. Biol. Chem. 272*, 23031−23036.
19. Ryle, M. J., Padmakumar, R., and Hausinger, R. P. (1999) *Biochemistry 38*, 15278−15286.
20. Ho, R. Y. N., Mehn, M. P., Hegg, E. L., Liu, A., Ryle, M. J., Hausinger, R. P., and Que, L., Jr. (2001) *J. Am. Chem. Soc. 123*, 5022−5029.
21. Pavel, E. G., Zhou, J., Busby, R. W., Gunsior, M., Townsend, C. A., and Solomon, E. I. (1998) *J. Am. Chem. Soc. 120*, 743−753.
22. Zhou, J., Kelly, W. L., Bachmann, B. O., Gunsior, M., Townsend, C. A., and Solomon, E. I. (2001) *J. Am. Chem. Soc. 123*, 7388−7398.
23. Elkins, J. M., Ryle, M. J., Clifton, I. J., Hotopp, J. C. D., Lloyd, J. S., Burzlaff, N. I., Baldwin, J. E., Hausinger, R. P., and Roach, P. L. (2002) *Biochemistry 41*, 5185−5192.
24. Gill, S. C., and von Hippel, P. H. (1990) *Anal. Biochem. 189*, 283.
25. Hitchman, M. L. (1978) *Chemical Analysis, Vol. 49: Measurement of Dissolved Oxygen*, Wiley, New York.
26. Bollinger, J. M., Jr., Tong, W. H., Ravi, N., Huynh, B. H., Edmondson, D. E., and Stubbe, J. (1994) *J. Am. Chem. Soc. 116*, 8015−23.
27. Ravi, N., Bollinger, J. M., Jr., Huynh, B. H., Stubbe, J., and Edmondson, D. E. (1994) *J. Am. Chem. Soc. 116*, 8007−8014.
28. Baldwin, J., Krebs, C., Ley, B. A., Edmondson, D. E., Huynh, B. H., and Bollinger, J. M., Jr. (2000) *J. Am. Chem. Soc. 122*, 12195−12206.
29. Arciero, D. M., Lipscomb, J. D., Huynh, B. H., Kent, T. A., and Münck, E. (1983) *J. Biol. Chem. 258*, 14981−14989.
30. Wolgel, S. A., Dege, J. E., Perkins-Olson, P. E., Juarez-Garcia, C. H., Crawford, R. L., Münck, E., and Lipscomb, J. D. (1993) *J. Bacteriol. 175*, 4414−4426.
31. Sturgeon, B. E., Burdi, D., Chen, S., Huynh, B. H., Edmondson, D. E., Stubbe, J., and Hoffman, B. M. (1996) *J. Am. Chem. Soc. 118*, 7551−7557.

32. Davydov, R., Kuprin, S., Gräslund, A., and Ehrenberg, A. (1994) *J. Am. Chem. Soc. 116*, 11120−11128.
33. Valentine, A. M., Tavares, P., Pereira, A. S., Davydov, R., Krebs, C., Hoffman, B. M., Edmondson, D. E., Huynh, B. H., and Lippard, S. J. (1998) *J. Am. Chem. Soc. 120*, 2190−2191.
34. Liu, K. E., Valentine, A. M., Wang, D., Huynh, B. H., Edmondson, D. E., Salifoglou, A., and Lippard, S. J. (1995) *J. Am. Chem. Soc. 117*, 10174−10185.
35. Debrunner, P. G. (1989) *Phys. Bioinorg. Chem. Ser. 4*, 137−234.
36. Simonneaux, G., Scholz, W. F., Reed, C. A., and Lang, G. (1982) *Biochim. Biophys. Acta 716*, 1−7.
37. Grapperhaus, C. A., Mienert, B., Bill, E., Weyhermüller, T., and Wieghardt, K. (2000) *Inorg. Chem. 39*, 5306−5317.
38. Rohde, J.-U., In, J.-H., Lim, M. H., Brennessel, W. W., Bukowski, M. R., Stubna, A., Münck, E., Nam, W., and Que, L., Jr. (2003) *Science 299*, 1037−1039.
39. Lim, M. H., Rohde, J.-U., Stubna, A., Bukowski, M. R., Costas, M., Ho, R. Y., Münck, E., Nam, W., and Que, L., Jr. (2003) *Proc. Natl. Acad. Sci. U.S.A., 100*, 3665−3670.
40. Zheng, H., Yoo, S. J., Münck, E., and Que, L., Jr. (2000) *J. Am. Chem. Soc. 122*, 3789−3790.
41. Shu, L., Nesheim, J. C., Kauffmann, K., Münck, E., Lipscomb, J. D., and Que, L., Jr. (1997) *Science 275*, 515−518.
42. Lee, D., Pierce, B., Krebs, C., Hendrich, M. P., Huynh, B. H., and Lippard, S. J. (2002) *J. Am. Chem. Soc. 124*, 3993−4007.
43. Brown, C. A., Pavlosky, M. A., Westre, T. E., Zhang, Y., Hedman, B., Hodgson, K. O., and Solomon, E. I. (1995) *J. Am. Chem. Soc. 117*, 715−732.
44. Meyer-Klaucke, W., Winkler, H., Schünemann, V., Trautwein, A. X., Nolting, H. F., and Haavik, J. (1996) *Eur. J. Biochem. 241*, 432−439.
45. Dutta, S., Peng, S.-M., and Bhattacharya, S. (2000) *Inorg. Chem. 39*, 2231−2234.
46. Barbaro, P., Bianchini, C., Linn, K., Mealli, C., Meli, A., Vizza, F., Laschi, F., and Zanello, P. (1992) *Inorg. Chim. Acta 198−200*, 31−56.
47. Barbaro, P., Bianchini, C., Mealli, C., and Meli, A. (1991) *J. Am. Chem. Soc. 113*, 3181−3183.

BI030011F